Analysis of a segmented q-plate tunable retarder for the generation of first order vector beams

JEFFREY A. DAVIS[1], NOBUYUKI HASHIMOTO[2], MAKOTO KURIHARA[2], ENRIQUE HURTADO[1], MELANIE PIERCE[1], MARÍA M. SÁNCHEZ-LÓPEZ[3], KATHERINE BADHAM[1], IGNACIO MORENO[4,*]

[1]*Department of Physics. San Diego State University, San Diego, CA 92182-1233, USA*
[2]*Development Division, Citizen Holdings Co., Ltd, Saitama 359-8511, Japan*
[3]*Instituto de Bioingeniería. Universidad Miguel Hernández, 03202 Elche, Spain*
[4]*Departamento de Ciencia de Materiales, Óptica y Tecnología Electrónica. Universidad Miguel Hernández, 03202 Elche, Spain*
**Corresponding author: i.moreno@umh.es*

http://dx.doi.org/10.1364/AO.54.009583

In this work we study a prototype *q*-plate segmented tunable liquid-crystal retarder device. It shows a large modulation range (5π radians for a wavelength of 633 nm and near 2π for 1550 nm), and large clear aperture of one-inch diameter. We analyze the operation of the *q*-plate in terms of Jones matrices and provide different matrix decompositions useful for its analysis, including the polarization transformations, the effect of the tunable phase-shift, and the effect of quantization levels (the device is segmented in 12 angular sectors). We also show a very simple and robust optical system capable of generating all polarization states on the first order Poincaré sphere. An optical polarization rotator and a linear retarder are used in a geometry that allows the generation of all states in the zero order Poincaré sphere simply by tuning two retardance parameters. We then use this system with the *q*-plate device to directly map an input arbitrary state of polarization to a corresponding first order vectorial beam. This optical system would be more practical for high speed and programmable generation of vector beams than other systems reported so far. Experimental results are presented. © 2015 Optical Society of America

OCIS codes: *(230.3720) Liquid-crystal devices, (230.5440) Polarization-selective devices, (120.5410) Polarimetry.*

http://dx.doi.org/10.1364/AO.99.099999

1. INTRODUCTION

Optical retarder elements with azimuthal rotation of the principal axes are receiving a great deal of attention in the last years due to their ability to create cylindrically polarized vector beams, and to transfer orbital angular momentum (OAM) to light [1]. This is the case of the *q*-plates [2,3] or the *s*-plates [4], which are half-wave retarders where the principal axis rotates with the azimuth angle. These devices can be fabricated with special liquid crystal patterns [5-9], or by means of local polarization transformation of metasurfaces [10].

These devices produce higher order cylindrically polarized vector fields with a polarization state that varies spatially with axial symmetry [11]. The two most common versions of these states are radially and azimuthally polarized light. They have been receiving a great attention because they can produce very small focal spots [12], or generate a longitudinal electric or magnetic field component upon focalization [13], as well as for their potential use in high-speed communication systems, where OAM and vector beams can be employed as additional degrees of freedom [14]. Such cylindrically polarized vector beams can be represented in the higher order Poincaré spheres [10,15-18], which are generalizations of the usual standard Poincaré sphere employed to describe a beam of light with uniform state of polarization [19]. The control of the input polarization can be used to generate different paths in the generalized Poincaré sphere, as it has been demonstrated using systems with rotatable half-wave and quarter-wave retarders [20]. In combination with other optical elements displayed on spatial light modulators, such plates can be used to generate Bessel beams with spatially varying states of polarizations [21].

In this work, we study a prototype segmented tunable *q*-plate device from Citizen Holdings Co [22]. This device shows a large modulation range (5π radians for λ=633 nm, 3π radians for λ=980 nm and almost 2π radians for the telecommunications wavelength of λ=1550 nm). The segmented structure (the device is segmented in 12 angular sectors) might be more suitable for lower cost production compared with the previously mentioned devices where the optical axis rotates continuously with the azimuth angle, while still providing more than 97.7% efficiency. The device has a large clear aperture of one-inch diameter. This is much larger than previously reported devices and makes this device very promising for combination with other liquid-crystal spatial light modulators (SLM), for the realization of optical elements that combine the polarization properties of the *q*-plate with the flexibility to create other patterns offered by SLMs.

We analyze the operation of the q-plate in terms of Jones matrices and provide different Jones matrix decompositions useful for its polarization action analysis, including the polarization transformations, and the effects of the tunable retardance. We also analyze the effects of the segmented angular sectors on the optical efficiency of the device. In addition, we examine the time response of the device as the driving voltage is changed and find some interesting effects. Experimental results are presented.

As stated previously, there is great interest in utilizing these devices to produce different channels in high-speed optical fiber multiplexing systems. In order to achieve the required modulation frequencies, it is necessary to switch the input polarization state at high speed. However, previous optical systems designed to control the input polarization state utilize rotatable retarders, which cannot be switched at such high speeds. Here, on the contrary, we demonstrate a very simple and robust optical system capable of generating all polarization states on the first order Poincaré sphere, which can be easily adapted for high speed switching. Our optical system consists of an optical polarization rotator and a linear retarder in a geometry that allows the generation of all states in the first order Poincaré sphere simply by tuning two retardance parameters that directly correspond to twice the ellipticity and twice the azimuth angles of the generated state of polarization. Our design is different from previously reported optical systems [20] because the angular positions of the elements remain fixed and the only adjustments are to the phase retardations for both retarders. In fact, electrically variable liquid crystal retarders [23] or electro-optic modulators [24] could be used to make the system fully programmable, high speed, and avoid any moving elements while obtaining Gigabit speeds. Experimental results are presented.

We organize the paper as follows: in Section 2, we briefly review the q-plate theory in terms of the Jones matrix formalism, and present some useful related matrix decompositions. Then, in Section 3 we study the characteristics of the Citizen q-plate, including its electrical tunability, operation at 632 nm, 980 nm and 1550 nm wavelengths, the efficiency of the segmented design and its time response. In Section 4 we show how the device can be used with our optical system to generate all beams in the first order Poincaré sphere. We describe the experimental system and show experimental results. Finally Section 5 includes the conclusions of the work.

2. REVIEW OF THE Q-PLATE THEORY

In this section we review the operation of the q-plate. We use the Jones matrix formalism and present some interesting decompositions useful for its comprehension. There are three aspects that we want to analyze in this paper related to the Citizen q-plate: retardance tunability, effect of the quantization, and its operation as an azimuthal rotator. While many of these studies have been addressed by other authors, some have not, and we feel that it would be valuable to the optical community to combine and review all of these into a single section of this work.

The q-plate consists of a phase plate retarder with retardance ϕ where the principal axis of the retarder follows q times the azimuthal angle θ. Therefore, its Jones matrix can be expressed as:

$$\mathbf{M}_q(\phi)=\mathbf{R}(-q\theta)\cdot\mathbf{W}(\phi)\cdot\mathbf{R}(+q\theta) \tag{1}$$

where

$$\mathbf{R}(\theta)=\begin{pmatrix}\cos\theta & \sin\theta\\ -\sin\theta & \cos\theta\end{pmatrix} \tag{2}$$

is the rotation matrix, and where:

$$\mathbf{W}(\phi)=\begin{pmatrix}e^{i\phi/2} & 0\\ 0 & e^{-i\phi/2}\end{pmatrix} \tag{3}$$

Note than Eq. (1) can be rewritten as:

$$\mathbf{M}_q(\phi)=\begin{pmatrix}\cos\left(\frac{\phi}{2}\right)-i\sin\left(\frac{\phi}{2}\right)\cos(2q\theta) & -i\sin\left(\frac{\phi}{2}\right)\sin(2q\theta)\\ -i\sin\left(\frac{\phi}{2}\right)\sin(2q\theta) & \cos\left(\frac{\phi}{2}\right)+i\sin\left(\frac{\phi}{2}\right)\cos(2q\theta)\end{pmatrix}$$
$$=\cos\left(\frac{\phi}{2}\right)\mathbf{I}-i\sin\left(\frac{\phi}{2}\right)\mathbf{M}_q(\phi=\pi) \tag{4}$$

where $\mathbf{I}$ stands for the identity matrix, and $\mathbf{M}_q(\phi=\pi)$ is the Jones matrix for the usual q-plate with a retardance of π radians given by [3]:

$$\mathbf{M}_q(\phi=\pi)=\begin{pmatrix}\cos(2q\theta) & \sin(2q\theta)\\ \sin(2q\theta) & -\cos(2q\theta)\end{pmatrix} \tag{5}$$

Equation (4) reveals that the retardance ϕ acts as a tuning parameter between these two matrices, with amplitude factors $\cos(\phi/2)$ and $\sin(\phi/2)$ respectively.

On the other hand, the matrix in Eq. (5) resembles the rotation matrix, but it is not. It can be decomposed as:

$$\mathbf{M}_q(\phi=\pi)=\mathbf{R}(-2q\theta)\cdot\mathbf{HWP} \tag{6}$$

where $\mathbf{HWP}=\mathbf{W}(\phi=\pi)=\mathrm{diag}(1,-1)$. This relation reveals that the q-plate tuned to π retardance acts as the combination of a pure polarization rotator with a rotation angle equal to $2q\theta$ and a vertically aligned half-wave retarder.

The usual case corresponds to q=1/2 and it is illustrated in Fig. 1(a). This is the case of our device. When the retardance is tuned to $\phi=\pi$, the actuation of the matrix in Eqs. (5)-(6) transforms horizontal linear polarization onto azimuthal polarization (Fig. 1(b)), vertical linear polarization onto radial polarization (Fig. 1(c)), and input circular polarization onto the opposite circular polarization plus an azimuthal phase (Fig. 1(d)).

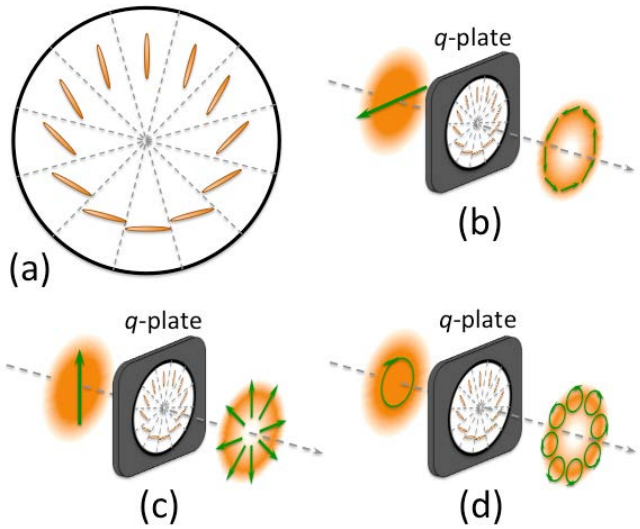

Fig. 1. (a) Structure of the segmented q=1/2 plate, with indication of the LC director orientation. It transforms (b) horizontal linear polarization into azimuthal polarization, (c) vertical linear polarization into radial polarization, and (c) circular polarization into the opposite circular polarization plus an azimuthal phase.

A. Tuning the retardance and its characterization

The use of a LC material allows the retardance to be tuned through an applied voltage, and adapt it to the operating wavelength. However, this requires an appropriate retardance characterization. In standard liquid crystal retarders, this is done by placing the device between

linear polarizers oriented at ±45 degrees to the LC director [25]. For *q*-plates this is not a practical solution because of the rotation of the liquid crystal director.

Instead, the retardance can be examined by generating and detecting left and right circularly polarized light (LCP and RCP). From Eq. (4) it is straightforward to derive that input RCP/LCP light ($E_{RCP/LCP}$) impinging the *q*-plate is transformed onto the following output:

$$E_{out} = \cos\left(\frac{\phi}{2}\right) E_{RCP/LCP} - i\sin\left(\frac{\phi}{2}\right) e^{\pm i2q\theta} E_{LCP/RCP} \quad (7)$$

which is a linear combination of RCP and LCP light. Also, as noted by many others, the output circular component that reversed its helicity with respect to the input beam, has additionally gained a helical phase charge of $\pm 2q\theta$. This helical phase corresponds to an orbital angular momentum (OAM) of $\pm 2q\hbar$ per photon, and it is the basis of the spin-to-orbital angular momentum conversion produced by the *q*-plate (the spin angular momentum (SAM) related to the circular polarization states is of $\pm\hbar$ per photon) [1].

Equation (7) shows that the transmitted intensity of the *q*-plate in between circular polarizers is given by:

$$I_T = I_0 \cos^2\left(\frac{\phi}{2}\right) \quad (8)$$

when the input and output polarizers have the same helicity (RCP to RCP, or LCP to LCP), where I_0 indicates the input intensity on the device. In the opposite case, where the input and output circular polarizers are the opposite (RCP to LCP and LCP to RCP), the transmission is given by

$$I_T = I_0 \sin^2\left(\frac{\phi}{2}\right) \quad (9)$$

In the literature [26,27], these expressions are characterized as similar to the Malus law, but are not derived to our knowledge, and this name is usually associated with the transmission through two linear polarizers.

B. Effect of the angular quantization of the segments

The prototype device, manufactured by Citizen Holdings Co, is composed of a number of sectors and it is useful to examine the efficiency of this design compared to a *q*-plate where the angle of wave plates varies continuously. This analysis can be done with the aid of a second useful decomposition that applies to the tuned *q*-plate Jones matrix in Eq. (5), which is obtained by applying Euler relations and ordering the elements as:

$$\mathbf{M}_q(\varphi=\pi) = \frac{1}{2}\exp(i2q\theta)\begin{pmatrix} 1 & -i \\ -i & -1 \end{pmatrix} + \frac{1}{2}\exp(-i2q\theta)\begin{pmatrix} 1 & i \\ i & -1 \end{pmatrix} = \exp(+i2q\theta)\mathbf{P}_{RCP\to LCP} + \exp(-i2q\theta)\mathbf{P}_{LCP\to RCP} \quad (10)$$

This shows that the tuned *q*-plate can be viewed as the combination of two circular polarizers, one $\mathbf{P}_{LCP\to RCP}$ transmitting LCP polarization, converting it onto RCP polarization, and adding a topological charge $\ell_{RCP} = +2q$, plus another circular polarizer $\mathbf{P}_{RCP\to LCP}$ transmitting RCP polarization, converting it onto LCP polarization, and adding the topological charge $\ell_{LCP} = -2q$. We used previously this type of decomposition to generate beams with different charges on RCP and LCP components by using a SLM [28].

This last decomposition can be used to easily analyze the effect of the quantization of the angular sectors. Note that the same theory that applied to quantized linear phase gratings and segmented spiral phase plates [29,30] can be applied to the exponential terms in Eq. (10). Therefore, $\mathbf{M'}_q(\phi=\pi)$, the Jones matrix describing the quantized version of Eq. (10) is given by:

$$\mathbf{M'}_q(\phi=\pi) = \mathbf{P}_{LCP\to RCP}\sum_n c_n \exp(+in2q\theta) + \mathbf{P}_{RCP\to LCP}\sum_n c_n \exp(-in2q\theta) = \sum_n c_n \mathbf{M}_{nq} \quad (11)$$

where c_n are the elements of the Fourier series of the quantized linear phase [30].

This analysis shows that higher order harmonic components raised by quantization correspond here to higher order *q*-plates $\mathbf{M}_{nq}$ with *q* values $q_n = nq$. In addition, the conversion efficiency for a segmented device for generating RCP from LCP (or the reverse) varies as $|c_1|^2 = \mathrm{sinc}^2(\pi/N)$, where $\mathrm{sinc}(x) = \sin(x)/x$, and would be 97.7% for a $N=12$ segmented device.

Although segmented *q*-plates have been reported earlier [31], the efficiency analysis of the device has been done with a scalar analysis of the power spiral spectrum [6]. This above equation represents an extension in the form of a Jones matrix spectrum of the angularly quantized *q*-plate. Note that an equivalent approach can be applied to a multi-elliptical core optical fiber [32], which can be used to generate vector beams, but also showing discrete patterns, just like the segmented *q*-plate.

3. EXPERIMENTS WITH THE CITIZEN Q-PLATE DEVICE

The *q*-plate is a prototype device from Citizen Holdings Co. [22] consisting of 12 liquid crystal segments as shown in FIg. 1(a) where the retardance of each segment can be varied using an applied voltage. The active diameter of the device is about 2.5 cm. Note that the phase decreases as the voltage increases. As described in section 2.A, the characterization of the retardance can be performed by measuring the conversion between circular polarizations. This conversion is complete when the phase of the *q*-plate acts as a half wave retarder.

In the experiments, light from a He-Ne laser was spatially filtered and collimated. The desired input circular polarization was generated using high quality linear polarizers and quarter-wave plates (Meadowlark Optics, models DPM-200-VIS and NQM-200-0633 respectively). The desired circular polarization state was detected using an equivalent system. The contrast ratio between cases where the desired input state was detected and when the opposite circular polarization state was detected was about 40,000/1. The transmitted light was either sent to a camera or focused onto a Newport Corp model 920 detector.

The retardance of the segments was adjusted using a 1 kHz square wave generated with a SIGLENT model SDG1025 signal generator. Figure 2(a) shows the results when LCP was incident onto the *q*-plate and RCP was detected. Maximum transmission is observed without applied voltage, indicating that the retardance is an odd multiple of π radians. When a voltage is applied to the device, then the LC director tilts and causes a reduction of the retardance. Results follow the expected oscillatory behavior of Eq. (9). More than two complete oscillations are observed, with the retardance decreasing towards zero as the voltage increased.

We see that the device is fabricated so that the retardance with no applied voltage is a half-wave multiple at this wavelength. The signal generator allows for precise generation of the applied voltage and we found the contrast ratio was reduced to about 400/1. This is partly due to the fact that we at SDSU did not mount the device onto a sufficiently flat surface. We believe that the contrast value could be improved by mounting the *q*-plate on a better flat surface. A tuning range over a retardance of 5π radians is demonstrated. We identified five voltage values: points A, C and E on Fig. 2(a) that

correspond to the ideal situation, where the *q*-plate is tuned to half-wave retardance ($\phi = 5\pi, \phi = 3\pi$ and $\phi = \pi$ respectively); while B and D correspond to full-wave retardance ($\phi = 4\pi$ and $\phi = 2\pi$ respectively).

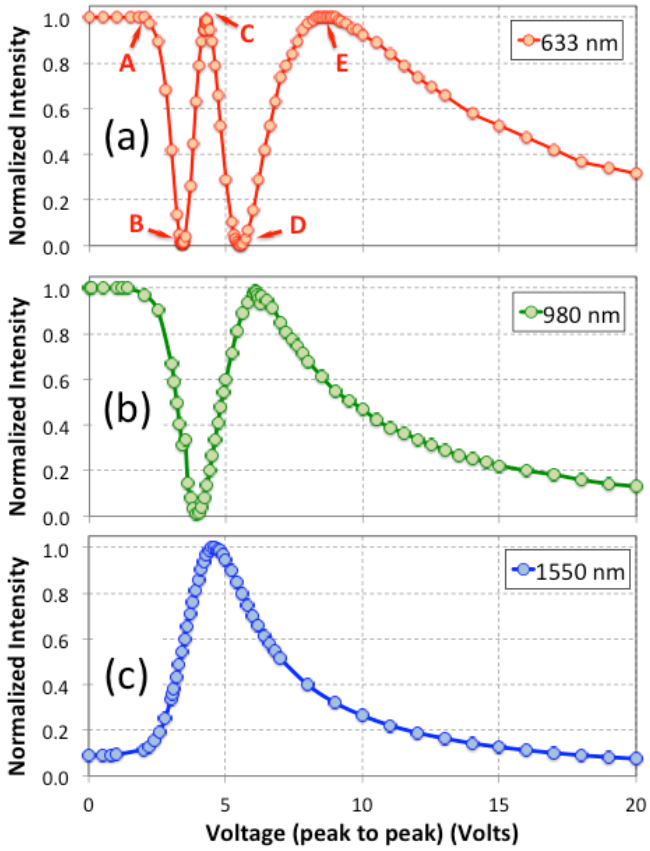

Fig. 2. Normalized transmission versus applied voltage of the *q*-plate between crossed circular polarizers (input LCP and detected RCP) for (a) λ=633 nm, (b) λ=980 nm and (c) λ=1550 nm.

Because of interest in using these devices for telecommunications applications, we also studied the operation at 980 nm and at 1550 nm. We used a B&K diode laser for the 980 nm wavelength and a New Focus tunable laser for the 1550 nm wavelength, both with optical fiber outputs. The light from the fiber was collimated with a 10 cm lens and then focused using a similar lens onto a Newport model 8184G infrared detector. In this case, we used Glan-Thompson polarizers and Soleil-Babinet (SB) compensators to operate at these wavelengths. The SB compensators were adjusted to act as quarter-wave plates for the operating wavelength, in order to build up the circular polarization generator and detector. The corresponding experimental results are shown in Figs. 2(b) and 2(c) respectively. The retardance for 980 nm is observed to reach 3π radians without applied voltage, while it is slightly less than 2π radians for 1550 nm. Again, these results show that the *q*-plate device achieves conversion of LCP into RCP for these wavelengths.

The temporal response is another interesting aspect in this kind of electro-optic device [27]. We selected voltages to switch between half-wave and full-wave retardance values as designated on Fig. 3(a). We used the red light of 633 nm wavelength. Interestingly different results were obtained when the device was driven to operate between different maxima and minima in Fig 2(a). This was done by amplitude modulating the signal generator. The carrier square signal of 1 KHz was amplitude modulated with two levels V_{high} and V_{low}, with frequency of 0.8 Hz. The signals measured on the detector are shown in Fig. 3.

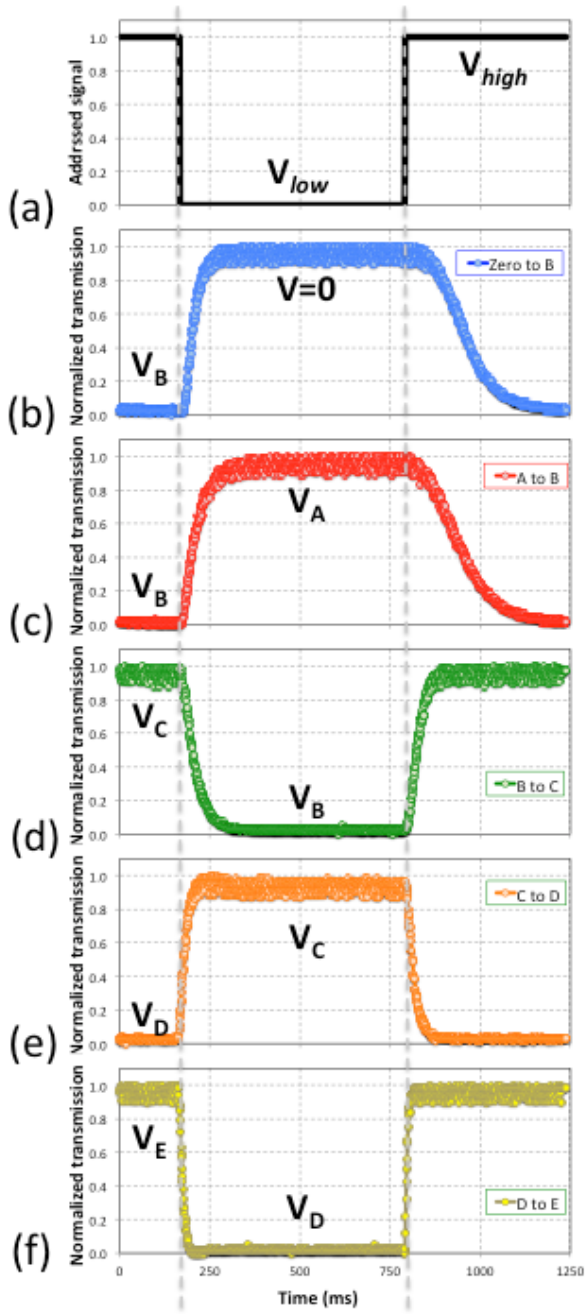

Fig. 3. Transmitted LCP to RCP conversion as functions of time as the applied voltage was amplitude modulated between selected points in Fig. 2(a). Wavelength is of 633 nm.

Figure 3(a) shows the electrical envelope signal, for comparison. In Fig. 3(b) the voltage varied between zero and 3.4 volts (point B in Fig. 2(a)), while in Fig. 3(c), the voltage varied between 1.8 volts and 3.4 volts (points A and B in Fig. 2(a)). We note the large delay in the response of the liquid crystal in the first case (45 ms rise and 150 ms fall). The rise and fall times are long because of the anchoring effects where the liquid crystal molecules are aligned parallel to the alignment layers at either end of the device. As the applied voltage increases, the molecules are initially tilted and are able to respond more quickly. This is shown in the other parts of the figure. In Figs. 3(d), 3(e) and 3(f) the applied voltage changed from 3.4 volts to 4.3 volts, from 4.3 volts to 5.4 volts, and from 5.4 volts to 8.4 volts, thus providing transitions between C, D and E in Fig. 2(a). The results in these figures are shown such that the central part corresponds always to the lower applied voltage V_{low}. This is why the rise and fall transitions are reversed in cases 3(d) and 3(f). In the latter case, the rise and fall times were

dramatically reduced to about 5 and 10 ms respectively. These results illustrate the importance of selecting the correct voltage levels when performing switching operations.

Next we discuss the generation of general vector beams on the Poincaré sphere using the q-plate and a specially designed polarization state generator.

4. GENERATION OF ELECTRIC FIELD VECTORS IN THE FIRST ORDER POINCARÉ SPHERE

Many proposed applications for these devices involve generation of various vector beams. In particular, the q=1/2 plate is useful for the generation of the vectorial beams in the first order Poincaré sphere. The classical zero order Poincaré sphere is a representation of the state of polarization defined in terms of the ellipticity (ε) and azimuth angles (α) (Fig. 4(a)). In this representation, these angles define a point with latitude 2ε and longitude 2α in the classical zero order Poincaré sphere, as shown in Fig. 4(b). The north and south poles are characterized by RCP and LCP circularly polarized light. The equator is characterized by linearly polarized light where the axis tilts as one moves longitudinally along the equator.

By contrast, first order vectorial beams are polarized beams where the state of polarization is spatially variant, with a constant ellipticity ε, but with an orientation that symmetrically rotates following the azimuth angle. These beams define the first order Poincaré sphere as shown in Fig. 4(c) [10,15-18]. The north and south poles are again characterized by RCP and LCP circularly polarized light, but with an additional azimuthal phase. The equator is characterized by ε=0 and

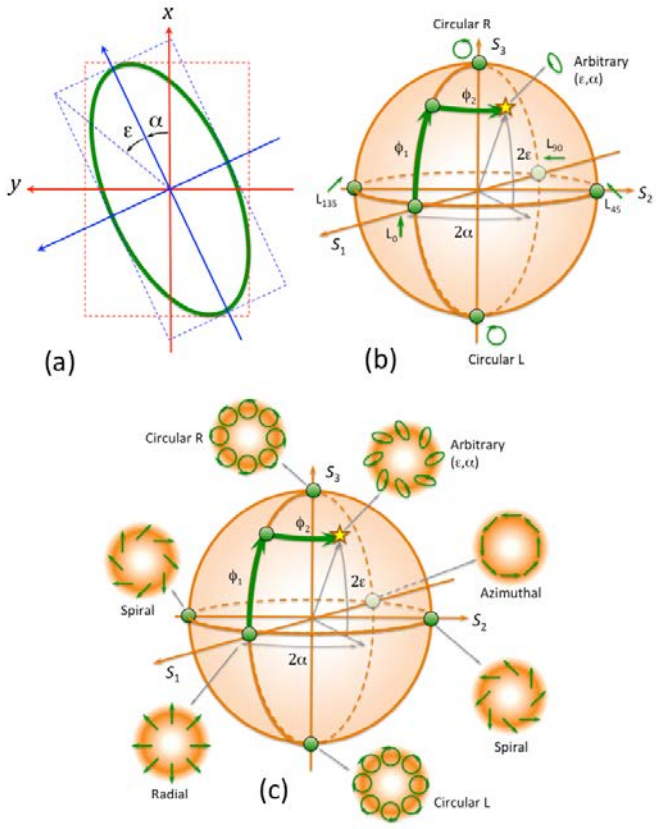

Fig. 4. (a) Representation of an arbitrary state of polarization with ellipticity and azimuth angles. (b) Zero order standard Poincaré sphere. (c) First higher order Poincaré sphere and representation of the six principal states, namely, radial, azimuthal, spiral, and circular states. In both cases, an indication of how to produce an arbitrary state with two linear retarders of phase shifts ϕ_1 and ϕ_2 (see Fig. 5) system is included.

has four cardinal points. At two opposite sides, we have the radially and azimuthally polarized beams. The other two cardinal points are characterized by spiral polarization states, where the spiral rotates in the clockwise or counterclockwise direction.

As with the zero order sphere, an arbitrary vectorial beam defines a point on the first order sphere with latitude defined by the ellipticity as 2ε, and longitude defined by 2α, where α denotes the azimuth of the state of polarization in the vertical direction. Fig. 4(c) shows the electric field patterns for these beams.

As stated earlier, many applications for these devices would require the capability to generate these beams at high speed. In a previous work [20], the polarized beams on the Poincaré sphere were generated using a sequence of quarter (Q) and half-wave plates (H) as QHQH. In order to generate various beams on the Poincaré sphere, the angles of the two H plates had to be adjusted. However, high speed switching of the polarization states is impractical with such a system.

As many of the applications for these vector beams might involve high speed or electronic tuning, we introduce here a more programmable system that is capable of high-speed generation of the desired states without any physical manipulation.

The optical system is illustrated in Fig. 5. It is composed of a linear polarizer oriented in the vertical direction, followed by a variable linear retarder (LR) and a variable optical rotator. The LR tunable phase axis is oriented at 45 degrees and has a retardance ϕ_1. The variable optical rotator system consists of two quarter-wave plates (QWP) oriented at +45 and -45 degrees, with another variable LR with tunable axis in the vertical direction and retardance ϕ_2 located between the two QWPs. The polarization rotation is equal to $\phi_2/2$ [33,34].

In this work, we have used two SB compensators as the variable linear retarders, but other devices like tunable liquid crystal retarders [23] could be used in order to make the system fully controlled from a computer eliminating the need for physical manipulation. High-speed operation (GHz) would be achieved by using electro-optic modulators [24]. The output beam illuminates the q-plate.

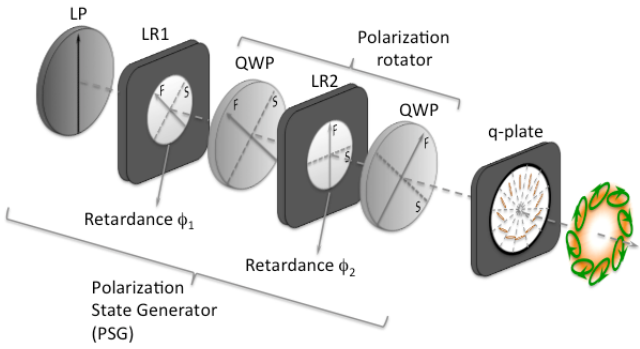

Fig. 5. Optical setup to generate arbitrary first order cylindrically polarized beams. LR: Variable linear retarder; QWP: Quarter-wave plate.

A very simple way to understand the system in Fig. 5 is to consider the transformations induced on the Poincaré sphere. This is visualized on Fig. 4(b). LR1 produces a rotation of the sphere of angle ϕ_1 around the S_2 axis. In addition, the QWP-LR2-QWP rotator system produces a rotation of the sphere of angle ϕ_2 around the S_3 axis. Since the input beam is vertically polarized, it corresponds to the point at the S_1 axis. Therefore, it is direct to deduce that the ellipticity and azimuth of the generated state are given by $2\varepsilon=\phi_1$ and $2\alpha=\phi_2$. Since this transformation is performed on the input beam, this rotation refers to the zero order Poincaré sphere in Fig. 4(b). Therefore,

the complete zero order Poincaré sphere can be covered by tuning the phase shifts ϕ_1 and ϕ_2.

Then, a device producing a pure azimuthal rotation $\mathbf{R}(-\theta)$ would transform this input beam onto the corresponding first order vectorial beam with the same coordinates on the first order Poincaré sphere, as shown in Fig. 4(c). Equation (6) indicates that the *q*-plate acts as the pure azimuthal retarder plus a half-wave retarder. Therefore, the *q*-plate could be converted into a pure azimuthal converter simply by adding a HWP in front of it. If this HWP is not added, the *q*-plate adds an extra 180 degrees rotation around the S_1 axis of the first Poincaré sphere, with respect to the pure azimuthal rotator.

The experimental system is similar to that discussed earlier. Light from the He-Ne laser is spatially filtered and collimated with a 37 cm focal length lens producing a uniform intensity plane wave over the *q*-plate device. A high quality (Meadowlark Optics, model DPM-200-VIS) linear polarizer is oriented vertical to the laboratory framework. Then, two SB compensators are used as LR devices. We used high quality wave-plates (Meadowlark Optics) in the system, as indicated in Fig. 5. The *q*-plate device was placed at the end.

We used three types of analyzers to examine the output beam: 1) a high quality linear polarizer, 2) two R and L circular polarizer sheets from Aflash Photonics (www.polarization.com), and finally, 3) a radial polarizer from Codixx (www.codixx.de). This last is a segmented polarizer with radial orientation of the transmission axis, which happens to have also 12 sectors [35]. The output beam is captured with a CCD detector. The results shown in Fig. 6 have been captured with the detector placed at a distance close to the *q*-plate device. In all cases, in the absence of the analyzers, the dark point in the center indicates the generation of the axial singularity.

First, the SB compensators were adjusted to zero retardance to produce the radially polarized beam out of linearly polarized input light. The corresponding experimental results are shown in the first row in Fig. 6. Each column shows: the CCD captures without the analyzer, with the linear analyzer oriented at 0, $\pm 45º$, and $90º$, and with RCP and LCP circular analyzers. The production of the radially polarized beam is verified by the presence of the dark horizontal line when the linear analyzer is oriented in the vertical direction, and by the rotation of this dark line with the analyzer. When circular analyzers are used, uniform intensity is obtained, as expected. Finally, when the radial analyzer is employed, we observe full transmission.

Then, the retardance ϕ_2 of the SB in the optical rotator system is varied in order to produce different vectorial beams along the equator of the first order Poincaré sphere. The images in the next three rows of Fig. 6 show the experimental results corresponding to the four cardinal points, namely radial, azimuthal and the two opposite spiral beams. In all cases, the correct generation of the polarization pattern is verified by noting the orientation of the dark line when the linear analyzer is employed. The uniform intensity when the circular analyzers are employed also confirms the results. It is interesting to note the result when $\phi_2=\pi$ and the radial polarizer is used. In this case, the azimuthal polarization is produced and it is completely cancelled by the radial polarizer.

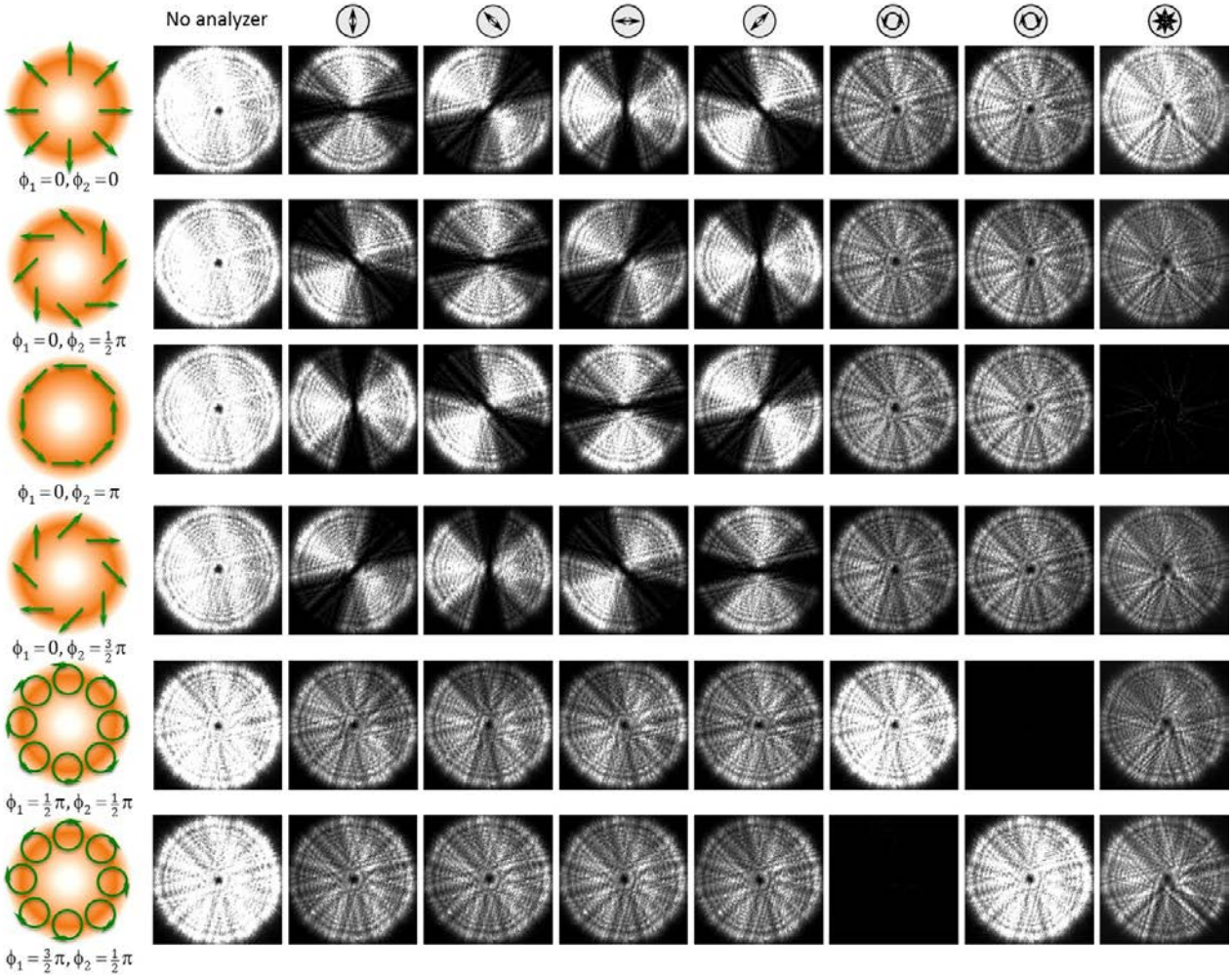

Fig. 6. Generation of vector beams in the first order Poincaré sphere. The polarization analyzer applied in each case is indicated on the top of the figure.

Finally, we changed the retardance of LR1 in the system and generated the vectorial beams corresponding to the poles in the first order Poincaré sphere. In this case, when $\phi_1=\pi/2$ is selected, RCP is produced at the input for the *q*-plate, which is transformed onto LCP vectorial beam (south pole of the first order Poincaré sphere). When $\phi_1=3\pi/2$ is selected, LCP is produced at the input for the *q*-plate, and it is transformed onto RCP vectorial beam (north pole of the first order Poincaré sphere). Experimental results are presented on the last two rows in Fig. 6. Note that now the intensity is uniform when a linear analyzer is employed, independently of its orientation. On the contrary, when the RCP and LCP circular analyzers are used, one shows a complete transmission, while the other completely blocks the beam. The radial polarizer also transmits with uniform half intensity.

5. CONCLUSIONS

In conclusion, we have investigated a new *q*-plate prototype device developed by Citizen Holdings Co., and applied it for the generation of arbitrary first order vectorial beams. We have characterized several parameters including the temporal response and the retardance variation with applied voltage at wavelengths of 633 nm, 980 nm, and the telecom wavelength of 1550 nm. We have reviewed the polarization transformations introduced by the *q*-plate, and found interesting decompositions of the Jones matrix for the device, to easily derive aspects like the effect of the retardance mismatch, or the quantization of the number of segments. We have identified the actuation of the *q*-plate as the combination of a pure azimuthal rotator and a half-wave retarder, and use it to transform an input beam with a homogeneous arbitrary state of polarization on the standard zero-order Poincaré sphere into a corresponding first-order vectorial beam onto the first order Poincaré sphere.

We demonstrate the approach using a very robust polarization state generator system consisting of a variable linear retarder oriented at 45º, and a variable optical rotator. This rotator is formed by another linear retarder placed between two QWPs. This polarization generator can produce states of polarization with arbitrary ellipticity and azimuth. The system is based on the retardance control of the two linear retarders, and no element must be rotated to achieve the full Poincaré sphere. Therefore it is very appropriate to be applied in telecommunications systems, where high speed is a requirement. In our system, we used two SB compensators as the two required linear retarders. However the system can be made fully programmable controlled from a computer using two liquid-crystal linear retarders, or with electro-optic retarders.

We believe that these results will be of interest to the community, particularly because the physical size of the device makes it compatible with programmable spatial light modulators.

Funding: MMSL and IM acknowledge financial support from Ministerio de Ciencia e Innovación from Spain (ref. FIS2012-39158-C02-02).

References

1. A. M. Yao and M. J. Padgett, "Orbital angular momentum: Origins, behavior and applications", Adv. Opt. Photon. **3**, 161–204 (2011).
2. A. Niv, Y. Gorodetski, V. Kleiner, and E. Hasman, "Topological spin–orbit interaction of light in anisotropic inhomogeneous subwavelength structures," Opt. Lett. **33**, 2910-2912 (2008).
3. L. Marrucci, C. Manzo, and D. Paparo, "Optical spin-to-orbital angular momentum conversion in inhomogeneous anisotropic media," Phys. Rev. Lett. **96**, 163905 (2006).
4. M. Beresna, M. Gecevičius, P. G. Kazansky, and T. Gertus, "Radially polarized optical vortex converter created by femtosecond laser nanostructuring of glass," Appl. Phys. Lett. **98**, 201101 (2011).
5. M. Stalder and M. Schadt, "Linearly polarized light with axial symmetry generated by liquid-crystal polarization converters," Opt. Lett. **21**, 1948-1950 (1996).
6. S. Slussarenko, A. Murauski, T. Du, V. Chigrinov, L. Marrucci, and E. Santamato, "Tunable liquid crystal q-plates with arbitrary topological charge," Opt. Express **19**, 4085-4090 (2011).
7. S. Nersisyan, N. Tabiryan, D. M. Steeves, and B. R. Kimball, "Fabrication of liquid crystal polymer axial waveplates for UV-IR wavelengths," Opt. Express **17**, 11926-11934 (2013).
8. S. Slussarenko, B. Piccirillo, V. Chigrinov, L. Marrucci, and E. Santamato, "Liquid crystal spatial-mode converters for the orbital angular momentum of light", J. Opt. **15**, 025406 (2013).
9. C. Loussert, K. Kushnir, and E. Brasseleta, "Q-plates micro-arrays for parallel processing of the photon orbital angular momentum", Appl. Phys. Lett. **105**, 121108 (2014).
10. Y. Liu, X. Ling, X. Yi, X. Zhou, H. Luo, and S. Wen, "Realization of polarization evolution on higher-order Poincaré sphere with metasurface," Appl. Phys. Lett. **104**, 191110 (2014).
11. Q. Zhan, "Cylindrical vector beams: From mathematical concepts to applications," Adv. Opt. Photon. **1**, 1–57 (2009).
12. S. Quabis, R. Dorn, M. Eberler, O. Glöckl and G. Leuchs, "Focusing light into a tighter spot," Opt. Commun. **179**, 1-7 (2000).
13. R. Dorn, S. Quabis, and G. Leuchs, "Sharper focus for a radially polarized light beams," Phys. Rev. Lett. **91**, 233901 (2003).
14. G. Milione, M. P. J. Lavery, H. Huang, Y. Ren, G. Xie, T. A. Nguyen, E. Karimi, L. Marrucci, D. A. Nolan, R. R. Alfano, and A. E. Willner, "4×20 Gbit/s mode division multiplexing over free space using vector modes and a q-plate mode (de)multiplexer," Opt. Lett. **40**, 1980-1983 (2015).
15. A. Holleczek, A. Aiello, C. Gabriel, C. Marquardt, G. Leuchs, "Classical and quantum properties of cylindrically polarized states of light," Opt. Express **19**, 9714-9736 (2011).
16. G. Milione, H. I. Sztul, D. A. Nolan, and R. R. Alfano, "Higher-order Poincaré sphere, Stokes parameters, and the angular momentum of light", Phys. Rev. Lett. **107**, 053601 (2011).
17. S. Chen, X. Zhou, Y. Liu, X. Ling, H. Luo, and S. Wen, "Generation of arbitrary cylindrical vector beams on the higher order Poincaré sphere," Opt. Lett. **39**, 5274-5276 (2014).
18. X. Yi, Y. Liu, X. Ling, X. Zhou, Y. Ke, H. Luo, S. Wen, and D. Fan, "Hybrid-order Poincaré sphere", Phys. Rev. A **91**, 023801 (2015).
19. D. Goldstein, *Polarized Light*, 2nd edition, Marcel Dekker Inc., New York (2003).
20. E. Karimi, S. Slussarenko, B. Piccirillo, L. Marrucci, and E. Santamato, "Polarization-controlled evolution of light transverse modes and associated Pancharatnam geometric phase in orbital angular momentum," Phys. Rev. A **81**, 053813 (2010).
21. G. Milione, A. Dudley, T.A. Nguyen, O. Chakraborty, E. Karimi, A. Forbes, and R.R. Alfano, "Measuring the self-healing of the spatially inhomogeneous states of polarization of vector Bessel beams", J. Opt. **17**, 035617 (2015).
22. N. Hashimoto, "Liquid crystal active optics and its application to laser microscopy", Invited Conferece, ref. 14SS-04, at the 9th International Conference on Optics-photonics Design & Fabrication, ODF '14, Itabashi, Tokyo (2014).
23. C. R. Fernández-Pousa, I. Moreno, J. A. Davis, and J. Adachi, "Polarizing diffraction-grating triplicators," Opt. Lett. **26**, 1651-1653 (2001)
24. L. Marrucci, C. Manzo, and D. Paparo, "Pancharatnam-Berry phase optical elements for wave front shaping in the visible domain: Switchable helical mode generation," Appl. Phys. Lett. **88**, 221102 (2006).
25. J. A. Davis, P. Tsai, D. M. Cottrell, and T. Sonehara, "Transmission variations in liquid crystal spatial light modulators caused by interference and diffraction effects," Opt. Eng. **38**, 1051-1057 (1999).
26. E. Karimi, B. Piccirillo, E. Nagali, L. Marrucci, and E. Santamato, "Efficient generation and sorting of orbital angular momentum eigenmodes of light by thermally tuned q-plates," Appl. Phys. Lett. **94**, 231124 (2009).
27. B. Piccirillo, V. D'Ambrosio, S. Slussarenko, L. Marrucci, and E. Santamato, "Photon spin-to-orbital angular momentum conversion via an electrically tunable q-plate," Appl. Phys. Lett. **97**, 241104 (2010).
28. I. Moreno, J. A. Davis, D. M. Cottrell, and R. Donoso, "Encoding high order cylindrically polarized light beams," Appl. Opt. **53**, 5493-5501 (2014).

29. C.-S. Guo, D.-M. Xue, Y.-J. Han, and J. Ding, "Optimal phase steps of multi-level spiral phase plates," Opt. Commun. **268**, 235–239 (2006).
30. N. Zhang, J. A. Davis, I. Moreno, D. M. Cottrell, and X.-C. Xuan, "Analysis of multilevel spiral phase plates using Dammann vortex sensing grating", Opt. Express **18**, 25987-25992 (2010).
31. J. Xin, K. Dai, L. Zhong, Q. Na, and C. Gao, "Generation of optical vortices by using spiral phase plates made of polarization dependent devices," Opt. Lett. **39**, 1984-1987 (2014).
32. G. Milione, H.I. Sztul, D. A. Nolan, J. Kim, M. Etienne, J. McCarthy, J. Wang, and R.R. Alfano, "Cylindrical vector beam generation from a multi elliptical core optical fiber", Proc. SPIE 7950, Complex Light and Optical Forces V, 79500K (2011)
33. C. Ye, "Construction of an optical rotator using quarter-wave plates and an optical retarder," Opt. Eng. **34**, 3031–3035 (1995).
34. J. A. Davis, D. E. McNamara, D. M. Cottrell and T. Sonehara, "Two-dimensional polarization encoding with a phase-only liquid crystal spatial light modulator," Appl. Opt. **39**, 1549-1554 (2000).
35. I. Moreno, J. Albero, J. A. Davis, D. M. Cottrell, and J. B. Cushing, "Polarization manipulation of radially polarized beams," Opt. Eng. **51**, 128003 (2012).